
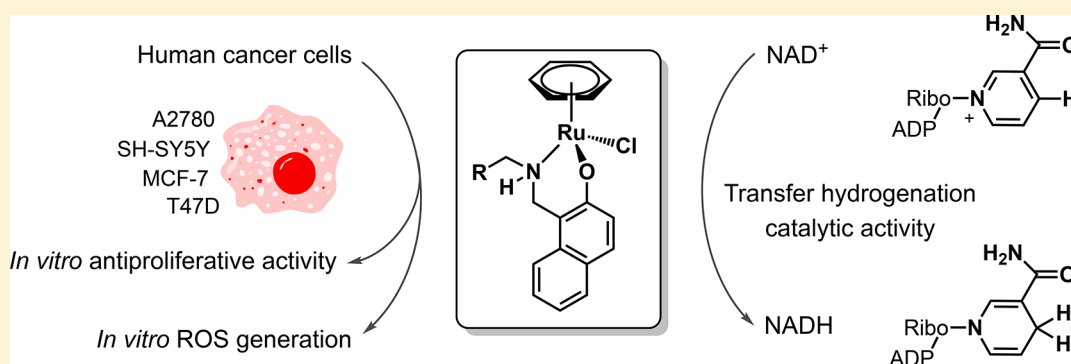


Anticancer Activity and Catalytic Potential of Ruthenium(II)–Arene Complexes with N,O-Donor Ligands

Mohammad Mehdi Haghdoust, Juliette Guard, Golara Golbaghi, and Annie Castonguay*

INRS-Institut Armand-Frappier, Université du Québec, 531 boul. des Prairies, Laval, Quebec H7V 1B7, Canada

 Supporting Information

ABSTRACT: The special ability of organometallic complexes to catalyze various transformations might offer new effective mechanisms for the treatment of cancer. Studies that report both the biological properties and the ability of metallic complexes to promote therapeutically relevant catalytic reactions are limited. Herein, we report the anticancer activity and catalytic potential of some ruthenium(II)–arene complexes bearing bidentate Schiff base ligands (**2a** and **2b**) and their reduced analogues (**5a** and **5b**, respectively). In comparison to their Schiff base counterparts **2a** and **2b**, we demonstrate that amine complexes **5a** and **5b** display (i) a higher *in vitro* antiproliferative activity on different human cancer cell lines, (ii) a lower rate of hydrolysis, and (iii) an improved initial catalytic rate for the reduction of NAD^+ to NADH . In contrast to their imine analogues **2a** and **2b**, we also show that amine complexes **5a** and **5b** induce the generation of intracellular reactive oxygen species (ROS) in MCF-7 breast cancer cells. Our results highlight the impact that a simple ligand modification such as the reduction of an imine moiety can have on both the catalytic and biological activities of metal complexes. Moreover, the ruthenium complexes reported here display some antiproliferative activity against T47D breast cancer cells, known for their *cis*-platin resistance.

■ INTRODUCTION

Catalytic metallodrugs are considered as promising candidates for overcoming drawbacks of current chemotherapies.¹ As they can potentially be administered in small doses and act via novel modes of action, they are likely to display low toxicities and circumvent the development of drug resistance. Thus, a better understanding of the factors that positively affect both the anticancer and catalytic activities of metal-based complexes could lead to the discovery of novel effective mechanisms for the treatment of cancer. Numerous low-molecular weight catalytic metallodrugs were reported to successfully promote specific biochemical transformations of importance.^{1,2} Of high interest are metal complexes that can undergo cellular internalization and catalytically produce reducing or oxidizing agents, leading to cell dysfunction/death by altering their redox status.³ Such an approach is promising for the development of new effective mechanisms for cancer therapy. Redox-modulating catalytic metallodrugs can induce cancer cell death by various mechanisms such as the formation of singlet oxygen,⁴ the dismutation of superoxide radicals,⁵ and the oxidation of thiols and/or transfer hydrogenation.^{2b,c,6} For instance, some

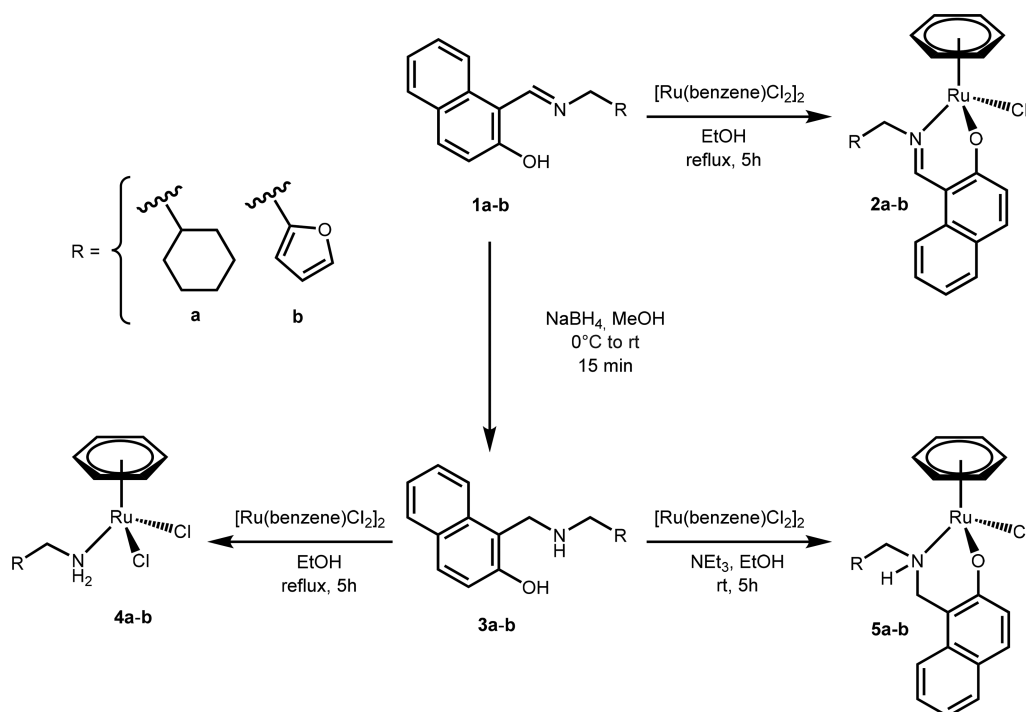
Mn(II) complexes with superoxide dismutase activity have entered clinical trials for the treatment of metastatic cancer.⁷

Ruthenium complexes hold promise as potential alternatives to platinum drugs currently used in various chemotherapy regimens.⁸ Because of their high catalytic activity for various oxidation/reduction reactions,⁹ they are excellent candidates for the modulation of the redox status of cancer cells. Notably, some Ru(II) complexes were reported to catalytically oxidize glutathione (GSH) to its corresponding disulfide (GSSG)¹⁰ under biological conditions, causing cancer cell death via oxidative stress.¹¹ A novel catalytic metallodrug system was recently reported using Noyori-type Ru(II) complexes to reduce NAD^+ to NADH in human cells in the presence of nontoxic doses of formate as a hydride source.^{2b} This catalytic reaction is believed to cause cancer cell death via reductive stress, a mechanism that has not yet been fully explored.

We recently reported the *in vitro* antiproliferative activity of Ru(II)–arene complexes bearing bidentate N,O-donor Schiff base ligands.¹² As numerous efficient ruthenium catalysts

Received: February 8, 2018

Scheme 1. Synthetic Route to Ruthenium Complexes



include secondary amines in their coordination sphere,¹³ we reasoned that the preparation of secondary amine analogues of some of these complexes could lead to species with enhanced catalytic and/or anticancer properties, and potentially help illuminating their possible mode(s) of action. Cyclohexane and furan-substituted ligands were selected for this study, not only because those substituents are among the most frequently used ring systems in small molecule drug design and their incorporation into the structure of transition metal complexes could potentially lead to interesting drug candidates,¹⁴ but also because of their great difference in lipophilicity. We know from previous studies that Ru(II)–arene complexes bearing cyclohexane and furan-substituted bidentate N,O-donor Schiff base ligands display a noticeable difference in their antiproliferative activity against cancer cells and that this difference could be attributed to their lipophilicity. For instance, a 4-fold improvement in antiproliferative activity against A2780 ovarian cancer cells was noted when a furyl substituent was replaced with a cyclohexyl. In this study, we were interested in assessing if this difference could affect the antiproliferative activity of analogous complexes with reduced ligands. Herein, we report the synthesis and characterization of similar Ru complexes with amine ligands (reduced corresponding imine ligands) and demonstrate that this small structural modification leads to complexes with improved anticancer and catalytic properties.

RESULTS AND DISCUSSION

Synthesis and Characterization. Ru(II)–arene complexes **2a** and **2b** bearing cyclohexane- and furan-substituted bidentate N,O-donor Schiff base ligands were readily obtained by mixing $[\text{Ru}(\text{benzene})\text{Cl}_2]_2$ and corresponding ligands **1a** and **1b** in ethanol,^{12,15} according to a detailed procedure we recently reported (Scheme 1).¹² Subsequent reduction of ligands **1a** and **1b** with NaBH_4 in methanol led to amine ligands **3a** and **3b**, respectively, in moderate yields (Scheme 1), which were characterized by nuclear magnetic resonance

(NMR), high-resolution electrospray ionization mass spectrometry (HR-ESI-MS) and elemental analysis. However, depending on the conditions used, this reduction reaction led to the formation of variable amounts of unexpected side products (Scheme S1). **3a** and **3b** could exclusively be obtained by allowing **1a** and **1b** to respectively react with NaBH_4 at room temperature for 15 min (addition at 0 °C), whereas increasing the reaction temperature or/and prolonging the reaction time resulted in the formation of a larger amount of side products.

When ligands **3a** and **3b** were allowed to react with $[\text{Ru}(\text{benzene})\text{Cl}_2]_2$ in refluxing ethanol for 5 h, the respective formation of target complexes **5a** and **5b** was not observed by NMR. Instead, the formation of unexpected ruthenium complexes **4a** and **4b** was detected, species arising from the breakage of the C–N bond of one of the ligands (Scheme 1). Nevertheless, complexes **5a** and **5b** could both be prepared in approximately 20% yield (Scheme 1) when the reaction was performed at room temperature, and with a more satisfactory yield (33–45%) when a base such as triethylamine was used in excess. The reduced form of the ligand in chiral complexes **5a** and **5b** was confirmed by ^1H NMR analysis, which showed a broad peak for the N–H proton and four distinctive peaks for the protons on the two adjacent carbons.¹⁶ Whereas only one set of signals could be observed in the ^1H NMR spectrum of **5a** in CDCl_3 , two diastereoisomers could be distinguished in the case of **5b**. The isolation of both species and the unambiguous assignment of their chiral centers were not pursued. Interestingly, complexes **5a** and **5b** were found to display a thermal stability higher than that of their corresponding ligands. For instance, no decomposition could be detected by ^1H NMR after refluxing a solution of complex **5a** or **5b** in ethanol (~15 mM) for 2 h. However, as expected from previous results, decomposition products were noted when **3a** or **3b** underwent the same treatment. The latter observation suggests that at elevated temperatures, the thermal cleavage of ligands **3a** and

3b might occur prior to their coordination to the ruthenium center, preventing the formation of **5a** and **5b**, respectively.

In addition to NMR and HR-ESI-MS, complexes **4a**, **5a**, and **5b** were also characterized by X-ray crystallography. Single crystals of complexes **4a** and **5a** were grown by slow evaporation of ethanol and chloroform solutions, respectively, whereas single crystals of complex **5b** were obtained by slow evaporation of a methanol/dichloromethane (1:1) solution.

Figure 1 presents an ORTEP view of the solid-state structure of

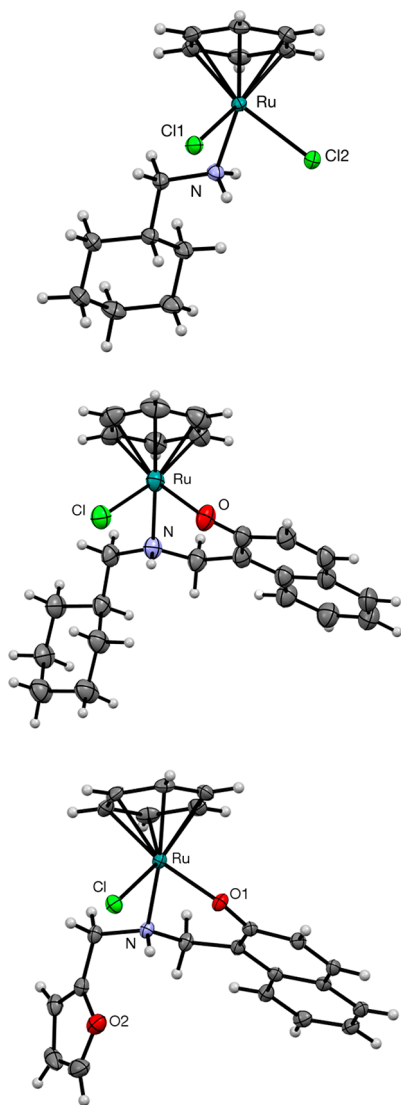


Figure 1. ORTEP diagrams of **4a** (top), **5a** (middle, $R_{Ru}S_N$ diastereomer shown), and **5b** (bottom, $R_{Ru}R_N$ diastereomer shown) with thermal ellipsoids drawn at the 50% probability level. For **5a**, the chloroform molecule has been omitted for clarity.

the three complexes, and a summary of their corresponding crystallographic data is provided in Table S1. Complex **4a** exhibits a distorted octahedral geometry (piano-stool structure) comprising an η^6 -coordinated benzene ring, one nitrogen-coordinated cyclohexane methylamine, and two chloride ligands. The crystal structure of similar ruthenium complexes was previously reported.¹⁷ Complexes **5a** and **5b** also display a Ru(II) pseudo-octahedral piano-stool configuration similar to that of previously reported corresponding Schiff base complexes.¹² The crystallographic data obtained for **5a** and

5b is consistent with their ligand being coordinated to the metal center in their reduced form, the corresponding C–N bond length values of 1.486(5) Å for **5a** and 1.485(3) for **5b** being characteristic of a single bond.¹⁸ The centrosymmetric space group ($P2_1/c$) in which both **5a** and **5b** crystallized suggests the presence of a racemic mixture in the solid state. In the case of **5b**, two types of crystals were obtained (orange needles and red blocks). When analyzed by X-ray crystallography, both were found to correspond to the same space group, asymmetric unit, and cell parameters.

The stability of metallic complexes has previously shown to greatly influence their anticancer activity.^{19,20} Unlike Schiff base complexes **2a** and **2b**, corresponding amine complexes **5a** and **5b** are stable when exposed to air for several weeks, as assessed by NMR and ESI-MS. However, as observed for their imine analogues, ultraviolet–visible (UV–vis) spectra of **5a** and **5b** display significant time-dependent changes with clear isosbestic points when dissolved in phosphate buffer [0.75% dimethyl sulfoxide (DMSO)], suggesting the occurrence of complex hydrolysis. Hydrolysis rate constants were calculated for complexes **5a** and **5b** using a pseudo-first-order kinetic model (Table S2) and were found to be approximately 10 times slower ($t_{1/2} = 80.7$ min for **5a**; $t_{1/2} = 56.3$ min for **5b**) than those corresponding to their Schiff base counterparts ($t_{1/2} = 9.3$ min for **2a**; $t_{1/2} = 4.2$ min for **2b**).¹² The latter observation can in part be explained by their different Ru–Cl bond strength, as observed for similar complexes.¹² Indeed, in their solid-state structure, the observed Ru–Cl bonds for **5a** [2.4019(9) Å] and **5b** [2.4196(6) Å] are slightly shorter than the corresponding bonds in the structures of their Schiff base counterparts, **2a** [2.427(2) Å] and **2b** [2.4395(6) Å], respectively.²¹ Furthermore, to estimate the stability of **5a** and **5b** during antiproliferative activity studies, solutions of complexes in water and aqueous phosphate buffer (0.75% DMSO) were kept at 37 °C for 48 h and then analyzed by ¹H NMR and ESI-MS. In phosphate buffer, complexes showed two new arene peaks at higher chemical shifts, which could be attributed to aquation and hydrolysis products: [Ru(arene)(L)(H₂O)] and [Ru(arene)(L)(OH)] complexes. Unfortunately, it was not possible to distinguish between those two species and the starting complex by MS, as peaks at m/z 448.20 and 432.27 were observed for **5a** and **5b**, respectively, corresponding to the mass of the ruthenium cation arising from the loss of a ligand (either Cl, H₂O, or OH). More complicated ¹H NMR and MS spectra were recorded in water alone. For example, after 48 h in water at 37 °C, complexes **5a** and **5b** displayed several peaks in the arene region suggesting improved stability of complexes in buffered solutions. Under all tested conditions, no DMSO/phosphate adduct(s) coordination could be observed by ¹H NMR or MS.

Antiproliferative Activity. The antiproliferative activity of ruthenium complexes **5a** and **5b** was evaluated against human breast carcinoma (MCF-7), human ovarian cancer cells (A2780), and human neuroblastoma (SH-SY5Y) and compared with the previously established activity of **2a** and **2b** against the same cell lines. Their cytotoxicity was assessed using the MTS assay after a 48 h exposure to each compound, and results are presented as IC₅₀ values in Table 1. For most cancer cell lines, amine complexes **5a** and **5b** exhibited antiproliferative activities higher than those of Schiff base complexes **2a** and **2b**. Complex **5a** was found to be the most cytotoxic compound against cancer cells, and as concluded from our previous studies of complexes **2a** and **2b**,¹² its superior cytotoxicity versus that of

Table 1. IC₅₀ Values Determined for Ruthenium Complexes 2a, 2b, 5a, and 5b and *cis*-Platin against Multiple Cell Lines

	IC ₅₀ (μM) ^a				
	A2780 ^b	SH-SY5Y ^b	MCF-7 ^b	T47D ^b	MCF-12A ^c
2a	30.4 ± 2.8 ^d	67.1 ± 0.7 ^d	88.7 ± 5.9 ^d	21.4 ± 0.8	37.9 ± 0.8
2b	135 ± 4 ^d	>150 ^d	>150 ^d	113 ± 11	105 ± 7
5a	8.9 ± 0.8	13.6 ± 3.6	49.8 ± 6.3	22.8 ± 4.3	59.3 ± 7.4
5b	50.1 ± 7.1	59.4 ± 7.3	108 ± 5	100 ± 6	111 ± 12
<i>cis</i> -platin	1.3 ± 0.4	4.1 ± 0.1	27.2 ± 3.3	>150	26.7 ± 3.0

^aInhibitory activity was determined by exposure of cell lines to each complex for 48 h and expressed as the concentration required to inhibit cell metabolic activity by 50% (IC₅₀). Errors correspond to the standard deviation of two to four independent experiments. ^bCancerous cell line. ^cNon-cancerous cell line. ^dResult reported previously.¹²

5b could be explained by its higher lipophilicity (cyclohexyl vs furan substituent) which might facilitate its cellular uptake. Interestingly, when the human breast T47D *cis*-platin resistant cancerous cell line²² was also treated with the same metallic complexes (Table 1), both types of complexes displayed a similar cytotoxicity. Importantly, T47D cells were found to be more sensitive to ruthenium treatment than to clinically approved *cis*-platin, as lower IC₅₀ values were noted when cells were treated with ruthenium complexes bearing either Schiff base or amine ligands. Moreover, when non-cancerous MCF-12A breast cells were treated with the same complexes, reduced amine complex 5a did not only display a toxicity lower than that of its Schiff base counterpart 2a, but did display a toxicity even lower than that of the widely used therapeutic agent *cis*-platin. Those preliminary results are in line with previous reports suggesting that ruthenium complexes could be considered as interesting alternative drug candidates for cancer patients who do not respond to *cis*-platin based treatments.²³

Catalytic Reduction of NAD⁺. We found of high interest to assess whether the ruthenium complexes reported here could promote the catalytic transfer hydrogenation of nicotinamide adenine dinucleotide (NAD⁺),^{2b} a coenzyme found in living cells. NAD plays a critical role in cellular metabolism and is involved in numerous intracellular redox reactions.²⁴ The ratio between its oxidized (NAD⁺) and reduced (NADH) forms is pivotal to the cell as significant shifts from the normal ratio change the cell redox status, causing an alteration in cell metabolism and leading to cell dysfunction.²⁵ As cancer cells are sensitive to changes in their redox balance,^{2b} catalysts able to modulate the intracellular NAD⁺/NADH ratio can provide a new strategy for the selective treatment of cancer.

The ability of complex 5a to promote the catalytic reduction of NAD⁺ to NADH was confirmed by UV-vis using sodium formate as the hydrogen donor (Scheme 2). Because the catalytic reduction of NAD⁺ to NADH with Ru(II) catalysts generally leads to very low TON and TOF values when the reaction is performed in water,^{2b,26} various conditions were initially used to confirm the catalytic nature of the system (Figure S1). Up to 4 TON could be observed after 1 h using 1

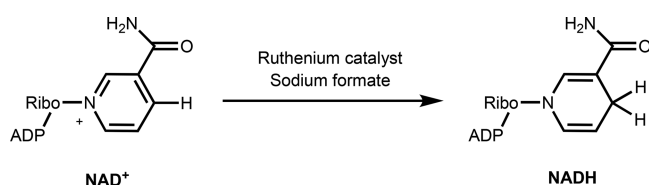
mol % 5a when a 1:1 water/methanol mixture was heated to 60 °C. It is important to note that because NADH is not thermally stable,²⁷ catalyst efficiency might be underestimated. To allow a comparison with previously reported systems,^{26b,c,28} the turnover frequency (TOF) of the catalyst was measured within the first 5 min of the reaction. Among the parameters tested, an improved catalytic activity was observed (Table 2) when

Table 2. Reduction of NAD⁺ Using Formate as the Hydride Source in the Presence of Complex 5a^a

entry	catalyst load (mol %)	solvent	temp (°C)	TOF (h ⁻¹) ^b
1	2	H ₂ O	37	1.12 ± 0.07
2	2	H ₂ O/MeOH (4:1)	37	3.14 ± 0.12
3	2	H ₂ O/MeOH (1:1)	37	3.7 ± 0.09
4	2	phosphate buffer ^c	37	2.39 ± 0.04
5	2	phosphate buffer	22	0.62 ± 0.05
6	2	phosphate buffer	45	4.29 ± 0.13
7	2	phosphate buffer	60	12.65 ± 0.53
8	0.5	phosphate buffer	37	2.12 ± 0.02
9	1	phosphate buffer	37	2.38 ± 0.05
10	4	phosphate buffer	37	1.21 ± 0.03
11	8	phosphate buffer	37	0.58 ± 0.06
12	16	phosphate buffer	37	0.31 ± 0.01

^aGeneral conditions: 8 mM NAD⁺, 350 mM HCOONa, 992 μL of solvent, 7.5 μL of DMSO, 5 min. ^bTurnover frequency defined as moles of product per mole of catalyst per hour. Errors correspond to the standard deviation of three independent experiments. ^cPhosphate buffer (0.1 M, pH 7) was used for experiments from entries 4–12.

reactions were performed in water/methanol mixtures (entries 1–4) or at higher temperatures (entries 5–7). When using different amounts of 5a under biologically relevant conditions (phosphate buffer, 37 °C, entries 4 and 8–12), the highest TOF obtained was found to be 2.4 h⁻¹, with a catalyst load of either 1 or 2 mol %. Interestingly, lower TOF values were observed when higher catalyst loads were used, suggesting a limited solubility of the catalyst in aqueous phosphate buffer and/or catalyst deactivation due to the formation of multi-nuclear metal clusters at these higher concentrations.^{19,29} A catalyst load of 1% was selected to assess the impact of the reduction of the Schiff base ligands on the reactivity of the different systems. Interestingly, amine complexes 5a and 5b were not only found to display higher antiproliferative activities (*vide supra*) compared to those of their imine analogues (2a and 2b, respectively) but to also display improved catalytic activities (Figure 2). For instance, TOF observed for complex 5b was found to be 4 times higher (1.62 ± 0.2) than the one noted for its corresponding Schiff base complex 2b (0.38 ± 0.09). The enhanced catalytic activity of amine complexes may

Scheme 2. Ruthenium-Catalyzed Reduction of NAD⁺ to NADH

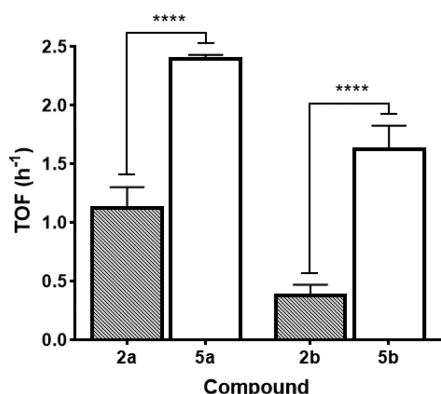


Figure 2. TOF values (moles of product per mole of catalyst per hour) for ruthenium complexes in the catalytic reduction of NAD^+ using formate as the hydride source. Conditions: 8 mM NAD^+ , 350 mM sodium formate, 992 μL of 0.1 M phosphate buffer (pH 7), 7.5 μL of DMSO, 75 μM catalyst, 37 $^\circ\text{C}$, 5 min. Error bars represent standard errors ($n = 3$). **** $P < 0.0001$.

be attributed to the stabilization of catalyst–substrate interactions through hydrogen bonding, which was previously hypothesized for similar hydrogen transfer systems.³⁰ Turnover frequencies (TOFs) from 0.38 to 2.39 h^{-1} (Figure 2) were noted, a range of activities that is higher than that of similar complexes with ethylenediamine^{26a} and bipyridine^{26b} ligands, and typically observed for some ruthenium–arene complexes with Noyori's chelating ligands [*N*-(2-aminoethyl)-sulfonamides].^{2b,31} For instance, the ruthenium(II) sulfonamide ethylenamine complex [(*p*-cym)Ru(TsEn)Cl] [TsEn = *N*-(2-aminoethyl)-4-methyl-benzenesulfonamide], the first ruthenium complex reported to catalyze the reduction of NAD^+ to NADH inside cancerous cells, was found to display a TOF value of 2.89 ± 0.08 under similar reaction conditions.^{2b} In contrast to a previous report indicating a direct correlation between the catalytic activity and the hydrolysis rate of ruthenium complexes for the reduction of NAD^+ ,^{26b} we noted a higher catalytic activity for ruthenium complexes with a lower rate of hydrolysis (Figure S2).

We investigated the ability of the complexes to catalyze the reduction reaction in living cells by assessing their antiproliferative activity against human cancer cell lines (T47D, A2780, SH-SY5Y, and MCF-7), in the presence of nontoxic doses of sodium formate (2–10 mM).^{2b} For all complexes, no significant change in their antiproliferative activity was noted when cells were co-treated with formate, suggesting that their anticancer activity could possibly take place via another (or multiple) mode(s) of action by interacting with other biomolecules. Transition metal complexes capable of catalyzing the interconversion of NAD^+ and NADH inside human cells are scarce^{2b,28–32} mainly because of the intracellular heterogeneous environment in which the catalyst must operate. For instance, Ru(II),^{26b,28b,31} Ir(III),^{28b,c,33} and Rh(III)^{26b,34} complexes were previously reported to catalyze the hydrogen transfer reaction between NAD^+ and NADH but could not operate after being exposed to cells.

ROS Generation. Inside each human living cell, a fine balance between reducing and oxidizing agents determines the cell redox status that plays a crucial role in cell survival.^{3,35} Similar to the catalytic reduction of NAD^+ to NADH that can cause modulation of the cell redox status, the overproduction of ROS may also lead to a disrupted cell redox balance, resulting

in oxidative stress and cell death.³⁶ The uncontrolled growth of cancer cells is often associated with increased ROS levels, making them more vulnerable to further ROS-generating insults than normal cells. Thus, the use of ROS-generating catalytic metallodrugs might be a promising strategy to selectively induce cancer cell death.³⁷ This strategy has been reported for some ruthenium^{10a} and osmium³⁸ complexes and successfully applied in a clinical trial with two manganese–porphyrin complexes for the treatment of metastatic colorectal cancer.⁷ Moreover, according to two reports that were published shortly after the submission of this paper, some Ru–arene transfer hydrogenation catalysts that are able to promote the reduction of intracellular NAD^+ can also lead to an increase of ROS levels within cancer cells.³⁹

The effect of ruthenium complexes and *cis*-platin on the *in vitro* generation of ROS in the breast cancer cell line MCF-7 was assessed using the DCFDA probe by evaluating intensity of fluorescence radiation emitted from the cells at 2 h intervals after incubation with the compounds at a concentration of 40 μM (Figure 3). Interestingly, a significant increase in the

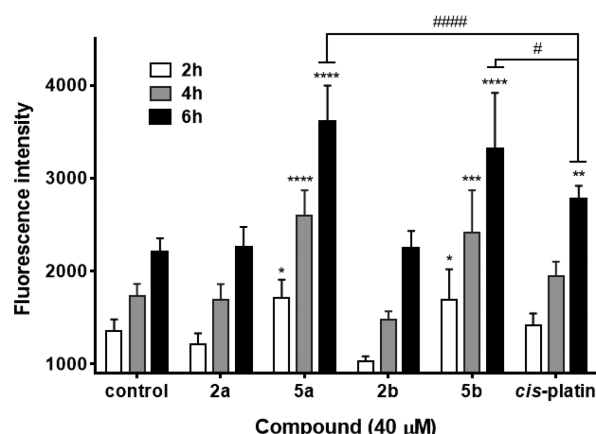


Figure 3. ROS level expressed as the fluorescence intensity of DCFHDA measured after treatment for 2, 4, and 6 h with compounds at a concentration of 40 μM (excitation at 485 nm and emission at 528 nm). Data are presented as means \pm standard deviations ($n = 5$). ** $P < 0.01$, *** $P < 0.001$, and **** $P < 0.0001$ vs cells exposed to the control (0.2% DMSO). # $P < 0.01$ and ##### $P < 0.0001$ vs *cis*-platin.

fluorescence intensity, proportional to ROS generation, was observed for samples treated with ruthenium complexes bearing amine ligands 5a and 5b, indicating their possible ability to modulate the cell redox status by *in vitro* ROS generation. However, a treatment with their imine counterparts 2a and 2b has not led to ROS induction inside cancerous cells, suggesting their lack of intracellular redox activity. In addition, a 6 h treatment with the same concentration of *cis*-platin, an anticancer agent known to generate ROS inside human cells,⁴⁰ also led to *in vitro* ROS induction but resulted in a fluorescence intensity slightly lower ($P < 0.01$) than that observed for ruthenium complexes 5a and 5b. Induction of intracellular ROS was previously reported as a cancer cell killing mechanism for several Ru(II)–arene complexes.^{10a,39,41}

CONCLUSION

Results obtained in the course of this study demonstrate the impact that a simple ligand modification such as the reduction of an imine moiety can have on the biological activity of metal complexes. In the case presented here, reduction of Schiff base

ligands to amines led to the formation of ruthenium complexes with the ability to induce accumulation of intracellular ROS. Moreover, results from this study also show that such small modifications can have a positive influence on the stability of metal complexes toward hydrolysis as well as on their ability to promote a catalytic reaction, such as the biologically relevant reduction of the coenzyme NAD⁺ to NADH. Besides, the ruthenium complexes reported here were found to display some antiproliferative activity against a human cell line known for its *cis*-platin resistance. Although the catalytic reaction investigated in this study (NAD⁺ reduction) was not evidently related to the antiproliferative activity of the reported ruthenium complexes, studies to assess if their anticancer activity can be linked to their ability to catalytically generate ROS *in vitro* are underway.

EXPERIMENTAL SECTION

General Remarks. All chemicals were purchased from commercial sources and used without further purification. [Ru(benzene)Cl₂]₂ was prepared and characterized according to a literature procedure,⁴² whereas ligands **1a** and **1b** and their corresponding complexes (**2a** and **2b**, respectively) were prepared according to procedures we recently reported.¹² The CellTiter 96 Aqueous One Solution Cell Proliferation Assay (MTS reagent) was purchased from Promega Corp. (Madison, WI). All reactions were performed under an inert atmosphere of nitrogen using Schlenk techniques. All solvents were dried using a solvent purification system (Pure Process Technology). BioTek Synergy HT and Tecan Infinite M1000 PRO microplate readers were used to record the absorbance (490 nm) of multiwell plates. NMR spectra (¹H, ¹³C{¹H}), COSY, HSQC, HMQC, and HMBC) were recorded on a 400 MHz Varian (Prometic Biosciences) or 500 MHz Bruker (Department of Chemistry, McGill University) spectrometers (25 °C). Chemical shifts (δ) and coupling constants are expressed in parts per million and hertz, respectively. ¹H and ¹³C{¹H} spectra were referenced to solvent resonances, and spectral assignments were confirmed by two-dimensional experiments. UV–vis spectra were recorded on a Cary 300 Bio UV–vis spectrometer. The purity (≥95%) of all complexes was confirmed by elemental analyses (Laboratoire d'Analyse Élémentaire, Département de Chimie, Université de Montréal). High-resolution and high-accuracy mass spectra (HR-ESI-MS) were recorded using an Exactive Orbitrap spectrometer from ThermoFisher Scientific (Department of Chemistry, McGill University). Diffraction measurements were performed on a SMART APEX II diffractometer equipped with a CCD detector, an Incoatec IMuS source (Cu), and a Quazar MX mirror (**5b**) or a Bruker Venture diffractometer (a liquid Ga Metal Jet source) equipped with a Photon 100 CMOS detector, Helios MX optics, and a Kappa goniometer (**4a** and **5a**) (Department of Chemistry, Université de Montréal). Column chromatography was performed using a Biotage Isolera One flash purification system with silica gel KP-Sil SNAP cartridges. All statistical analyses were performed using GraphPad Prism 6.01 software. Outliers were identified and removed from the analysis using the Rout method (*Q* < 5%). Analysis of variance was used to test the significance of the difference between the means, and a *P* value of <0.05 was considered statistically significant.

General Procedure for the Synthesis of **3a and **3b**.** NaBH₄ (0.060 g, 1.59 mmol, ~2 equiv) was added to an ice-cooled solution of Schiff base ligand **1** (1 equiv) in methanol (7 mL), and the reaction mixture was kept in an ice bath for 5 min. The ice bath was then removed, and the reaction mixture was allowed to stir for an additional 15–20 min until the solution became colorless. The reaction was quenched with water (10 mL, Milli-Q), and the resulting slurry was stirred vigorously for 30 min at room temperature. After the filtration of the reaction mixture and several washings with water (Milli-Q), a white solid was obtained and dried in a desiccator.

Ligand **3a.** **1a** (0.200 g, 0.75 mmol). Yield: 98%. ¹H NMR (400 MHz, CDCl₃): δ 7.80 (d, ³J_{H,H} = 8.6 Hz, 1H, *H*_{naphthyl}), 7.75 (d, ³J_{H,H} = 8.1 Hz, 1H, *H*_{naphthyl}), 7.68 (d, ³J_{H,H} = 8.8 Hz, 1H, *H*_{naphthyl}), 7.43 (m,

1H, *H*_{naphthyl}), 7.28 (m, 1H, *H*_{naphthyl}), 7.09 (d, ³J_{H,H} = 8.8 Hz, 1H, *H*_{naphthyl}), 4.47 (s, 2H, naphthyl-CH₂-N), 2.62 (d, ³J_{H,H} = 6.6 Hz, 2H, cyclohexyl-CH₂-N), 1.84–1.66 (m, 5H, *H*_{cyclohexyl}), 1.55 (m, 1H, *H*_{cyclohexyl}), 1.35–1.07 (3H, m, *H*_{cyclohexyl}), 1.06–0.87 (2H, m, *H*_{cyclohexyl}). ¹³C{¹H} NMR (100 MHz, CDCl₃): δ 157.2 (1C, *C*_{naphthyl}), 132.5 (1C, *C*_{naphthyl}), 129.1 (1C, *C*_{naphthyl}), 129.0 (1C, *C*_{naphthyl}), 128.5 (1C, *C*_{naphthyl}), 126.4 (1C, *C*_{naphthyl}), 122.4 (1C, *C*_{naphthyl}), 121.0 (1C, *C*_{naphthyl}), 119.7 (1C, *C*_{naphthyl}), 112.1 (1C, *C*_{naphthyl}), 56.1 (1C, cyclohexyl-CH₂-N), 48.1 (1C, naphthyl-CH₂-N), 37.8, 31.4, 26.6, 26.1 (6C, *C*_{cyclohexyl}). HR-ESI-MS: *m/z* (+) found 270.18 [*M* + *H*]⁺ (calcd 270.18). Anal. Calcd (%) for C₁₈H₂₃NO: C, 80.26; H, 8.61; N, 5.20. Found: C, 80.55; H, 9.29; N, 5.21.

Ligand **3b.** **1b** (0.200 g, 0.80 mmol). Yield: 77%. ¹H NMR (400 MHz, CDCl₃): δ 7.79–7.72 (m, 3H, *H*_{naphthyl}), 7.46–7.41 (m, 2H, 1H, *H*_{naphthyl} + 1H, *H*_{furyl}), 7.32–7.27 (m, 1H, *H*_{naphthyl}), 7.13 (d, ³J_{H,H} = 8.8 Hz, 1H, *H*_{naphthyl}), 6.35 (m, 1H, *H*_{furyl}), 6.29 (m, 1H, *H*_{furyl}), 4.42 (s, 2H, naphthyl-CH₂-N), 3.88 (s, 2H, furyl-CH₂-N). ¹³C{¹H} NMR (100 MHz, CDCl₃): δ 156.8 (1C, *C*_{naphthyl}), 151.7 (1C, *C*_{furyl}), 142.5 (1C, *C*_{furyl}), 132.5 (1C, *C*_{naphthyl}), 129.2 (1C, *C*_{naphthyl}), 128.8 (1C, *C*_{naphthyl}), 128.4 (1C, *C*_{naphthyl}), 126.2 (1C, *C*_{naphthyl}), 122.4 (1C, *C*_{naphthyl}), 121.0 (1C, *C*_{naphthyl}), 119.4 (1C, *C*_{naphthyl}), 111.5 (1C, *C*_{naphthyl}), 110.3 (1C, *C*_{furyl}), 108.4 (1C, *C*_{furyl}), 45.8 (1C, naphthyl-CH₂-N), 44.4 (1C, furyl-CH₂-N). HR-ESI-MS: *m/z* (+) found 254.11 [*M* + *H*]⁺ (calcd 254.11); Anal. Calcd (%) for C₁₆H₁₅NO₂: C, 75.87; H, 5.97; N, 5.53. Found: C, 76.14; H, 6.39; N, 5.56.

Synthesis of **4a.** One hundred milligrams of [Ru(benzene)Cl₂]₂ (2 mmol) and 107 mg of **3a** (0.40 mmol, 2 equiv) were refluxed in 15 mL of ethanol for 4 h. The reaction mixture was filtered through a small pad of Celite, and a slow evaporation of the filtrate yielded **4a** as orange needle-shaped crystals that were collected and washed with cold ethanol and diethyl ether. Yield: 15%. ¹H NMR (400 MHz, CD₂Cl₂): δ 5.61 (s, 6H, *η*⁶-benzene), 3.08–2.93 (m, 2H, CH₂), 2.88 (br, 2H, NH₂), 1.84–1.68 (m, 4H, *H*_{cyclohexyl}), 1.70–1.64 (m, 1H, *H*_{cyclohexyl}), 1.52–1.37 (m, 1H, *H*_{cyclohexyl}), 1.32–1.09 (m, 3H, *H*_{cyclohexyl}), 1.02–0.87 (m, 2H, *H*_{cyclohexyl}). ¹³C{¹H} NMR (100 MHz, CD₂Cl₂): δ 83.3 (6C, *η*⁶-benzene), 57.0 (1C, CH₂), 41.2, 31.0, 26.8, 26.2 (6C, *C*_{cyclohexyl}). HR-ESI-MS: *m/z* (+) found 364.01 [*M* + *H*]⁺ (calcd 364.01). Anal. Calcd (%) for C₁₃H₂₁Cl₂NRu: C, 42.98; H, 5.83; N, 3.86. Found: C, 43.49; H, 6.07; N, 3.84.

General Procedure for the Synthesis of **5a and **5b**.** A mixture of [Ru(benzene)Cl₂]₂ (1 equiv), corresponding reduced ligand (2.5 equiv), and triethylamine (6.1 equiv) was stirred in 15 mL of dry ethanol (or acetonitrile) at room temperature for 3 h, which resulted in the formation of an orange-red precipitate that was collected by filtration and washed with acetonitrile, ethanol, and diethyl ether.

Complex **5a.** 64 mg of [Ru(benzene)Cl₂]₂ (0.13 mmol), 86 mg of **3a** (0.32 mmol), and 109 μL of triethylamine (0.78 mmol). Yield: 45%. ¹H NMR (400 MHz, CDCl₃): δ 7.69 (d, ³J_{H,H} = 8.0 Hz, 1H, *ArH*), 7.48 (t, ³J_{H,H} = 10.1 Hz, 2H, *ArH*), 7.40 (m, 2H, *ArH*), 7.18 (m, 1H, *ArH*), 5.40 (s, 6H, *η*⁶-benzene), 4.29 (m, 2H, naphthyl-CH₂-N), 3.64 (m, 1H, cyclohexyl-CH₂-N), 3.44 (m, 1H, cyclohexyl-CH₂-N), 3.29 (br, 1H, CH₂-NH-CH₂), 2.03 (m, 1H, N-CH₂-CH_{cyclohexyl}), 0.87–1.80 (m, 10H, *H*_{cyclohexyl}). ¹³C{¹H} NMR (100 MHz, CDCl₃): δ 166.2 (1C, *C*_{Ar}), 132.4 (1C, *C*_{Ar}), 128.7 (1C, *C*_{Ar}), 127.6 (1C, *C*_{Ar}), 126.8 (1C, *C*_{Ar}), 126.0 (1C, *C*_{Ar}), 125.1 (1C, *C*_{Ar}), 121.0 (1C, *C*_{Ar}), 119.0 (1C, *C*_{Ar}), 111.9 (1C, *C*_{Ar}), 82.4 (6C, *η*⁶-benzene), 65.8 (2C, N-CH₂-cyclohexyl), 52.9 (naphthyl-CH₂-N), 35.0 (1C, N-CH₂-CH_{cyclohexyl}), 31.5, 29.6, 26.1, 25.9, 25.2 (6C, *C*_{cyclohexyl}). HR-ESI-MS: *m/z* (+) found 484.09 [*M* + *H*]⁺ (calcd 484.09); Anal. Calcd (%) for C₂₄H₂₈Cl₂NRu·H₂O: C, 57.53; H, 6.04; N, 2.80. Found: C, 58.34; H, 6.00; N, 2.99.

Complex **5b.** 64 mg of [Ru(benzene)Cl₂]₂ (0.13 mmol), 81 mg of **3b** (0.32 mmol), and 109 μL of triethylamine (0.78 mmol). Yield: 33%. ¹H NMR (500 MHz, CDCl₃, major isomer): δ 7.67 (d, ³J_{H,H} = 7.67 Hz, 1H, *H*_{naphthyl}), 7.48 (m, 2H, 1H, *H*_{naphthyl} + 1H, *H*_{furyl}), 7.42–7.34 (m, 3H, *H*_{naphthyl}), 7.17 (ddd, *J* = 8.0, 5.6, 2.4 Hz, 1H, *H*_{naphthyl}), 6.49 (d, ³J_{H,H} = 3.2 Hz, 1H, *H*_{furyl}), 6.40 (dd, ³J_{H,H} = 3.2, 1.9 Hz, 1H, *H*_{furyl}), 5.42 (s, 6H, *η*⁶-benzene), 4.97 (dd, *J* = 14.4, 2.2 Hz, 1H, CH₂), 4.52–4.35 (m, 2H, CH₂), 4.09 (dd, ³J_{H,H} = 15.2, 2.9 Hz, 1H, CH₂), 3.62 (br, 1H, CH₂-NH-CH₂). ¹H NMR (500 MHz, CDCl₃, minor isomer): δ 7.64 (d, ³J_{H,H} = 8.8 Hz, 1H, *ArH*), 7.32 (dd, ³J_{H,H} = 13.1, 4.2 Hz, 1H,

ArH), 6.54–6.50 (m, 2H, furyl), 5.31 (s, 6H, η^6 -benzene), 4.69 (dd, $^3J_{\text{H,H}} = 14.5, 6.6$ Hz, 1H, CH₂), 4.20 (dd, $^3J_{\text{H,H}} = 14.5, 6.6$ Hz, 1H, CH₂), 3.90 (m, 1H, CH₂), 3.48–3.38 (m, 1H, CH₂). Peaks of five aromatic hydrogens and the hydrogen of the N–H bond overlap with those of the major isomer. $^{13}\text{C}\{^1\text{H}\}$ NMR (125 MHz, CDCl₃): δ 166.5 (1C, C_{Ar}), 150.3 (1C, C_{Ar}), 143.4 (1C, C_{Ar}), 132.5 (1C, C_{Ar}), 128.7 (1C, C_{Ar}), 127.8 (1C, C_{Ar}), 127.0 (1C, C_{Ar}), 126.2 (1C, C_{Ar}), 125.1 (1C, C_{Ar}), 121.3 (1C, C_{Ar}), 119.4 (1C, C_{Ar}), 112.4 (1C, C_{Ar}), 111.1 (1C, C_{furyl}), 111.0 (1C, C_{furyl}), 82.6 (6C, η^6 -benzene), 54.2 (1C, CH₂), 53.1 (1C, CH₂). HR-ESI-MS: m/z (+) found 468.03 [M + H]⁺ (calcd 468.03). Anal. Calcd (%) for C₂₂H₂₀ClNO₂Ru·H₂O: C, 54.49; H, 4.57; N, 2.89. Found: C, 55.04; H, 4.25; N, 2.95.

X-ray Crystallography. Cell refinement and data reduction were performed using APEX2. Absorption corrections were applied using SADABS. Structures were determined by direct methods using SHELXS-97 and refined on F^2 by full-matrix least squares using SHELXL-97 or SHELXL-2014. All non-hydrogen atoms were refined anisotropically, whereas hydrogen atoms were refined isotropically on calculated positions using a riding model.⁴³

Hydrolysis. A stock solution (7.5 μL) of the complexes in DMSO (20 mM) was added directly to 992 μL of phosphate buffer (0.1 M, pH 7) in a UV–vis cuvette to reach a final complex concentration of 150 μM . The absorbance was monitored using UV–vis spectroscopy at 5 min intervals over 2 h at 297 K. Plots of the change in absorbance (at the wavelength corresponding to the maximum change in UV–vis spectra) versus time were fitted to the equation for pseudo-first-order kinetics using GraphPad Prism 6.01 software. Reaction rate constants ($K_{\text{H}_2\text{O}}$) and half-lives ($t_{1/2}$) were determined by the software and expressed as means \pm the standard deviation of three independent experiments.

Catalytic Reduction of NAD⁺. A stock solution (7.5 μL) of the complexes in DMSO (10 mM), 100 μL of a stock solution of sodium formate in water (3.5 M), and 732 μL of phosphate buffer (0.1 M, pH 7) were introduced into a UV–vis cell. The solution was monitored by UV–vis spectroscopy (250–600 nm) until no further change in the absorbance spectrum was observed, indicating that the hydrolysis reaction had reached equilibrium. Then, 160 μL of a stock solution of NAD⁺ in water (50 mM) was added to the UV–vis cell, and formation of NADH was monitored by repeated measurements of the absorbance at $\lambda = 340$ nm ($\epsilon = 6230 \text{ M}^{-1} \text{ cm}^{-1}$)^{28a} over a period of 60 min. For instance, in a typical catalytic experiment, final concentrations of Ru complex, NAD⁺, and sodium formate were 75 μM , 8 mM, and 350 mM, respectively (1:107:4667). Turnover frequency (TOF) values were determined by measuring turnover numbers (TONs, moles of product per mole of catalyst) for the initial 5 min of the catalytic reaction and are presented as means \pm the standard deviation of three independent experiments.

Cell Culture. The protocols used for biological studies were approved by the Institutional Research Ethics Committee of INRS-Institut Armand-Frappier. MCF-7 and A2780 cells were routinely grown in a Roswell Park Memorial Institute medium (RPMI-1640) supplemented with 10% fetal bovine serum (FBS) and 1% penicillin/streptomycin. ATCC-formulated RPMI-1640 supplemented with 0.2 unit/mL bovine insulin and 10% fetal bovine serum was used as the base medium for the T47D cell line. The complete growth medium for SH-SY5Y was an equal volume mixture of minimum essential medium and Ham's F12 nutrient mixture supplemented with sodium pyruvate (50 mg/L), 1% penicillin/streptomycin, and 15% FBS. The MCF-12A cells were grown in a DMEM/Ham's F12 (1:1) medium (containing L-glutamine, 15 mM HEPES, and sodium bicarbonate) supplemented with human EGF (20 ng/mL), cholera toxin (100 ng/mL), bovine insulin (10 ng/mL), hydrocortisone (500 ng/mL), 1% penicillin/streptomycin, and 5% horse serum. All components of culture media were purchased from Gibco, Invitrogen, and Sigma. Cell lines were grown as adherent monolayers in a humidified atmosphere of 5% CO₂ and 95% air at 37 °C. These cells were passaged two or three times per week at ~70–80% confluency by harvesting with trypsin and EDTA and seeding at a 1:4 to 1:10 ratio into 75 cm² flasks. Cells were used up to 10 passages after being thawed.

MTS Assays. Cell culture-treated 96-well plates (Sarstedt) were used to seed 5000 (A2780), 10000 (MCF-7, T47D, and MCF-12A), or 30000 (SH-SY5Y) cells per well. Plates were preincubated with the drug free medium at 37 °C (5% CO₂) for 24 h. Stock solutions of the test compounds in DMSO (10 or 20 mM) were diluted in complete culture medium to give final concentrations in the range of 1–150 μM (the maximum DMSO content did not exceed 0.75%). Medium was removed from wells, and 100 μL aliquots of these dilutions were added to each well for a drug exposure period of 48 h. Then, 20 μL of MTS reagent [3-(4,5-dimethylthiazol-2-yl)-5-(3-carboxymethoxyphenyl)-2-(4-sulfophenyl)-2H-tetrazolium bromide] was added to each well. The optical density, directly proportional to the cell metabolic activity, was quantified at 490 nm using a multiwell plate reader, and the antiproliferative activity was calculated by comparison to positive (25% DMSO) and negative controls (untreated wells). IC₅₀ values, concentrations that inhibit cell metabolic activity by 50%, were determined from concentration–effect curves by interpolation. This assay was performed in two to four independent sets of experiments, each experiment with four to six replicates per concentration level.

In Vitro ROS Generation. MCF-7 cells were seeded into Corning black side clear bottom 96-well plates (20000 cells/well) and grown overnight in complete medium. The medium was removed, and cells were washed with 100 μL of phenol red free RPMI-1640 and loaded with a 100 μL solution of 20 μM DCFDA in phenol red free RPMI-1640 (0.1% DMSO) for 45 min at 37 °C. After loading, unincorporated dye was removed by washing with 100 μL of phenol red free RPMI-1640. Compounds were freshly dissolved in DMSO (20 mM), diluted in phenol red free RPMI-1640 containing 1% FBS serum, and added to the cells to a final concentration of 40 μM . Fluorescence measurements were taken using a microplate reader by a 485/20 nm excitation and 528/20 nm emission filter pair from the bottom every 2 h for a total of 6 h (PMT sensitivity setting of 55). The experiment was performed in five replicates, and 20 μM H₂O₂ was used as a positive control.

■ ASSOCIATED CONTENT

● Supporting Information

The Supporting Information is available free of charge on the ACS Publications website at DOI: 10.1021/acs.inorgchem.8b00346.

Scheme S1, Tables S1 and S2, Figures S1 and S2, ¹H and ¹³C{¹H} NMR spectra, and references (PDF)

Accession Codes

CCDC 1558368–1558369 and 1821535 contain the supplementary crystallographic data for this paper. These data can be obtained free of charge via www.ccdc.cam.ac.uk/data_request/cif, or by emailing data_request@ccdc.cam.ac.uk, or by contacting The Cambridge Crystallographic Data Centre, 12 Union Road, Cambridge CB2 1EZ, UK; fax: +44 1223 336033.

■ AUTHOR INFORMATION

Corresponding Author

*E-mail: annie.castonguay@iaf.inrs.ca.

ORCID

Annie Castonguay: 0000-0001-5705-6353

Notes

The authors declare no competing financial interest.

■ ACKNOWLEDGMENTS

This work was supported by INRS-Institut Armand-Frappier, the Natural Sciences and Engineering Research Council of Canada (Discovery Grant), the Fonds de Recherche en Santé du Québec (Établissement de Jeunes Chercheurs), the Canada Foundation for Innovation (John Evans Leaders Fund), and the Armand-Frappier Foundation (Banque Nationale Scholarship

to G.G.). The authors thank Prof. David Chatenet, Prof. Isabelle Plante, and Prof. Yves St-Pierre for providing the human cancer cell lines used in this study. Finally, the authors also thank Prof. Nicolas Doucet and Prof. Charles Ramassamy for providing access to their instruments.

REFERENCES

- (1) Yu, Z.; Cowan, J. A. Catalytic Metallo-drugs: Substrate-Selective Metal Catalysts as Therapeutics. *Chem. - Eur. J.* **2017**, *23*, 14113–14127.
- (2) (a) Hocharoen, L.; Cowan, J. A. Metallotherapeutics: Novel Strategies in Drug Design. *Chem. - Eur. J.* **2009**, *15*, 8670. (b) Soldevila-Barreda, J. J.; Romero-Canelón, I.; Habtemariam, A.; Sadler, P. J. Transfer Hydrogenation Catalysis in Cells as a New Approach to Anticancer Drug Design. *Nat. Commun.* **2015**, *6*, 6582–6591. (c) Coverdale, J. P. C.; Romero-Canelón, I.; Sanchez-Cano, C.; Clarkson, G. J.; Habtemariam, A.; Wills, M.; Sadler, P. J. Asymmetric Transfer Hydrogenation by Synthetic Catalysts in Cancer Cells. *Nat. Chem.* **2018**, *10*, 347–354.
- (3) Trachootham, D.; Lu, W.; Ogasawara, M. A.; Valle, N. R.-D.; Huang, P. Redox Regulation of Cell Survival. *Antioxid. Redox Signaling* **2008**, *10*, 1343–1374.
- (4) Josefsen, L. B.; Boyle, R. W. Photodynamic Therapy and the Development of Metal-Based Photosensitisers. *Met.-Based Drugs* **2008**, *2008*, 1–23.
- (5) Batinic-Haberle, I.; Tovmasyan, A.; Roberts, E. R. H.; Vujaskovic, Z.; Leong, K. W.; Spasojevic, I. SOD Therapeutics: Latest Insights into Their Structure-Activity Relationships and Impact on the Cellular Redox-Based Signaling Pathways. *Antioxid. Redox Signaling* **2014**, *20*, 2372–2415.
- (6) Soldevila-Barreda, J. J.; Sadler, P. J. Approaches to the Design of Catalytic Metallo-drugs. *Curr. Opin. Chem. Biol.* **2015**, *25*, 172–83.
- (7) Karlsson, J. O. G.; Ignarro, L. J.; Lundström, I.; Jynge, P.; Almén, T. Calmangafodipir [$\text{Ca}_4\text{Mn}(\text{DPDP})_5$], Mangafodipir (MnDPDP) and MnPLED with Special Reference to Their SOD Mimetic and Therapeutic Properties. *Drug Discovery Today* **2015**, *20*, 411–421.
- (8) Model List of Essential Medicines. World Health Organization. http://www.who.int/entity/medicines/publications/essentialmedicines/20th_EML2017_FINAL_amendedAug2017.pdf?ua=1 (accessed March 2017).
- (9) Gunanathan, C.; Milstein, D. Bond Activation and Catalysis by Ruthenium Pincer Complexes. *Chem. Rev.* **2014**, *114*, 12024–12087.
- (10) (a) Dougan, S. J.; Habtemariam, A.; McHale, S. E.; Parsons, S.; Sadler, P. J. Catalytic Organometallic Anticancer Complexes. *Proc. Natl. Acad. Sci. U. S. A.* **2008**, *105*, 11628–11633. (b) Bugarcic, T.; Habtemariam, A.; Deeth, R. J.; Fabbiani, F. P. A.; Parsons, S.; Sadler, P. J. Ruthenium(II) Arene Anticancer Complexes with Redox-Active Diamine Ligands. *Inorg. Chem.* **2009**, *48*, 9444–9453. (c) Giannini, F.; Furrer, J.; Süß-Fink, G.; Clavel, C. M.; Dyson, P. J. Synthesis, Characterization and *In vitro* Anticancer Activity of Highly Cytotoxic Trithiolato Diruthenium Complexes of the Type $[(\eta^6\text{-}p\text{-Me-C}_6\text{H}_4\text{Pr})_2\text{Ru}_2(\mu_2\text{-SR}^1)_2(\mu_2\text{-SR}^2)]^+$ Containing Different Thiolato Bridges. *J. Organomet. Chem.* **2013**, *744*, 41–48. (d) Ibaño, A.-F.; Gras, M.; Therrien, B.; Süß-Fink, G.; Zava, O.; Dyson, P. J. Thiolato-Bridged Arene–Ruthenium Complexes: Synthesis, Molecular Structure, Reactivity, and Anticancer Activity of the Dinuclear Complexes $[(\text{arene})_2\text{Ru}_2(\text{SR})_2\text{Cl}_2]$. *Eur. J. Inorg. Chem.* **2012**, *2012*, 1531–1535.
- (11) Franco, R.; Cidlowski, J. A. Apoptosis and Glutathione: Beyond an Antioxidant. *Cell Death Differ.* **2009**, *16*, 1303–1314.
- (12) Haghdoost, M.; Golbaghi, G.; Létourneau, M.; Patten, S. A.; Castonguay, A. Lipophilicity-Antiproliferative Activity Relationship Study Leads to the Preparation of a Ruthenium(II) Arene Complex with Considerable *In vitro* Cytotoxicity against Cancer Cells and a Lower *In vivo* Toxicity in Zebrafish Embryos Than Clinically Approved Cis-Platin. *Eur. J. Med. Chem.* **2017**, *132*, 282–293.
- (13) (a) Ito, M.; Ootsuka, T.; Watari, R.; Shiibashi, A.; Himizu, A.; Ikariya, T. Catalytic Hydrogenation of Carboxamides and Esters by Well-Defined Cp^*Ru Complexes Bearing a Protic Amine Ligand. *J. Am. Chem. Soc.* **2011**, *133*, 4240–4242. (b) Dub, P. A.; Gordon, J. C. The Mechanism of Enantioselective Ketone Reduction with Noyori and Noyori-Ikariya Bifunctional Catalysts. *Dalton Trans.* **2016**, *45*, 6756–6781. (c) Noyori, R.; Hashiguchi, S. Asymmetric Transfer Hydrogenation Catalyzed by Chiral Ruthenium Complexes. *Acc. Chem. Res.* **1997**, *30*, 97–102.
- (14) Taylor, R. D.; MacCoss, M.; Lawson, A. D. G. Rings in Drugs. *J. Med. Chem.* **2014**, *57*, 5845–5859.
- (15) (a) Govender, P.; Renfrew, A. K.; Clavel, C. M.; Dyson, P. J.; Therrien, B.; Smith, G. S. Antiproliferative Activity of Chelating N,O- and N,N-Ruthenium(II) Arene Functionalised Poly(Propyleneimine) Dendrimer Scaffolds. *Dalton Trans.* **2011**, *40*, 1158–1167. (b) Maroto-Díaz, M.; Elie, B. T.; Gomez-Sal, P.; Perez-Serrano, J.; Gomez, R.; Contel, M.; Javier de la Mata, F. Synthesis and Anticancer Activity of Carbosilane Metallo-dendrimers Based on Arene Ruthenium(II) Complexes. *Dalton Trans.* **2016**, *45*, 7049–7066. (c) Matsinha, L. C.; Malatji, P.; Hutton, A. T.; Venter, G. A.; Mapolie, S. F.; Smith, G. S. Water-Soluble Half-Sandwich Ru(II)–Arene Complexes: Synthesis, Structure, Electrochemistry, DFT Studies, and Aqueous Phase Hydroformylation of 1-Octene. *Eur. J. Inorg. Chem.* **2013**, *2013*, 4318–4328. (d) Matsinha, L. C.; Mapolie, S. F.; Smith, G. S. Synthesis and Characterization of Mono- and Binuclear Iminopyridyl and Salicylaldimine Ru(II)–Arene Complexes. *Polyhedron* **2013**, *53*, 56–61.
- (16) Everaere, K.; Mortreux, A.; Bulliard, M.; Brussee, J.; van der Gen, A.; Nowogrocki, G.; Carpentier, J.-F. (β -Amino alcohol)(arene)-ruthenium(II)-Catalyzed Asymmetric Transfer Hydrogenation of Functionalized Ketones – Scope, Isolation of the Catalytic Intermediates, and Deactivation Processes. *Eur. J. Org. Chem.* **2001**, *2001*, 275–291.
- (17) (a) Sortais, J.-B.; Pannetier, N.; Holuigue, A.; Barloy, L.; Sirlin, C.; Pfeffer, M.; Kyritsakas, N. Cyclometalation of Primary Benzyl Amines by Ruthenium(II), Rhodium(III), and Iridium(III) Complexes. *Organometallics* **2007**, *26*, 1856–1867. (b) Tyagi, D.; Rai, R. K.; Dwivedi, A. D.; Mobin, S. M.; Singh, S. K. Phosphine-Free Ruthenium–Arene Complex for Low Temperature One-Pot Catalytic Conversion of Aldehydes to Primary Amides in Water. *Inorg. Chem. Front.* **2015**, *2*, 116–124. (c) Tyagi, D.; Binnani, C.; Rai, R. K.; Dwivedi, A. D.; Gupta, K.; Li, P.-Z.; Zhao, Y.; Singh, S. K. Ruthenium-Catalyzed Oxidative Homocoupling of Arylboronic Acids in Water: Ligand Tuned Reactivity and Mechanistic Study. *Inorg. Chem.* **2016**, *55*, 6332–6343. (d) Bacchi, A.; Cantoni, G.; Granelli, M.; Mazza, S.; Pelagatti, P.; Rispoli, G. Hydrogen Bond Optimization Via Molecular Design for the Fabrication of Crystalline Organometallic Wheel-and-Axle Compounds Based on Half-Sandwich Ru(II) Units. *Cryst. Growth Des.* **2011**, *11*, 5039–5047. (e) Cheng, B.; Tehrani, A. A.; Hu, M.-L.; Morsali, A. Supramolecular Assemblies of Ru(II) Organometallic Half-Sandwich Complexes. *CrystEngComm* **2014**, *16*, 9125–9134.
- (18) Allen, F. H.; Kennard, O.; Watson, D. G.; Brammer, L.; Orpen, A. G.; Taylor, R. Tables of Bond Lengths Determined by X-Ray and Neutron Diffraction. Part 1. Bond Lengths in Organic Compounds. *J. Chem. Soc., Perkin Trans. 2* **1987**, S1–S19.
- (19) Crabtree, R. H. Deactivation in Homogeneous Transition Metal Catalysis: Causes, Avoidance, and Cure. *Chem. Rev.* **2015**, *115*, 127–150.
- (20) Waterman, K. C.; Adami, R. C. Accelerated Aging: Prediction of Chemical Stability of Pharmaceuticals. *Int. J. Pharm.* **2005**, *293*, 101–125.
- (21) Wang, F.; Habtemariam, A.; van der Geer, E. P. L.; Fernández, R.; Melchart, M.; Deeth, R. J.; Aird, R.; Guichard, S.; Fabbiani, F. P. A.; Lozano-Casal, P.; Oswald, I. D. H.; Jodrell, D. I.; Parsons, S.; Sadler, P. J. Controlling Ligand Substitution Reactions of Organometallic Complexes: Tuning Cancer Cell Cytotoxicity. *Proc. Natl. Acad. Sci. U. S. A.* **2005**, *102*, 18269–18274.
- (22) (a) Ang, W. H.; Khalaila, I.; Allardyce, C. S.; Juillerat-Jeanneret, L.; Dyson, P. J. Rational Design of Platinum(IV) Compounds to Overcome Glutathione-S-Transferase Mediated Drug Resistance. *J. Am. Chem. Soc.* **2005**, *127*, 1382–1383. (b) Nieves-Neira, W.; Pommier, Y. Apoptotic Response to Camptothecin and 7-Hydrox-

ystaurosporine (UCN-01) in the 8 Human Breast Cancer Cell Lines of the NCI Anticancer Drug Screen: Multifactorial Relationships with Topoisomerase I, Protein Kinase C, Bcl-2, p53, MDM-2 and Caspase Pathways. *Int. J. Cancer* **1999**, *82*, 396–404.

(23) (a) Aird, R. E.; Cummings, J.; Ritchie, A. A.; Muir, M.; Morris, R. E.; Chen, H.; Sadler, P. J.; Jodrell, D. I. *In Vitro* and *in Vivo* Activity and Cross Resistance Profiles of Novel Ruthenium (II) Organometallic Arene Complexes in Human Ovarian Cancer. *Br. J. Cancer* **2002**, *86*, 1652. (b) Groessl, M.; Zava, O.; Dyson, P. J. Cellular Uptake and Subcellular Distribution of Ruthenium-Based Metallodrugs under Clinical Investigation Versus Cis-platin. *Metallomics* **2011**, *3*, 591–599.

(24) Christensen, C. E.; Karlsson, M.; Winther, J. R.; Jensen, P. R.; Lerche, M. H. Non-Invasive in-Cell Determination of Free Cytosolic [NAD(+)]/[NADH] Ratios Using Hyperpolarized Glucose Show Large Variations in Metabolic Phenotypes. *J. Biol. Chem.* **2014**, *289*, 2344–2352.

(25) Teodoro, J. S.; Rolo, A. P.; Palmeira, C. M. The NAD Ratio Redox Paradox: Why Does Too Much Reductive Power Cause Oxidative Stress? *Toxicol. Mech. Methods* **2013**, *23*, 297–302.

(26) (a) Yan, Y. K.; Melchart, M.; Habtemariam, A.; Peacock, A. F. A.; Sadler, P. J. Catalysis of Regioselective Reduction of NAD⁺ by Ruthenium(II) Arene Complexes under Biologically Relevant Conditions. *JBIC, J. Biol. Inorg. Chem.* **2006**, *11*, 483–488. (b) Haquette, P.; Talbi, B.; Barilleau, L.; Madern, N.; Fosse, C.; Salmain, M. Chemically Engineered Papain as Artificial Formate Dehydrogenase for NAD(P)H Regeneration. *Org. Biomol. Chem.* **2011**, *9*, 5720–5727. (c) Canivet, J.; Süß-Fink, G.; Štěpnička, P. Water-Soluble Phenanthroline Complexes of Rhodium, Iridium and Ruthenium for the Regeneration of NADH in the Enzymatic Reduction of Ketones. *Eur. J. Inorg. Chem.* **2007**, *2007*, 4736–4742.

(27) Wu, J. T.; Wu, L. H.; Knight, J. A. Stability of NAPH: Effect of Various Factors on the Kinetics of Degradation. *Clin. Chem.* **1986**, *32*, 314–319.

(28) (a) Steckhan, E.; Herrmann, S.; Ruppert, R.; Dietz, E.; Frede, M.; Spika, E. Analytical Study of a Series of Substituted (2,2'-Bipyridyl)(Pentamethylcyclopentadienyl)Rhodium and -Iridium Complexes with Regard to Their Effectiveness as Redox Catalysts for the Indirect Electrochemical and Chemical Reduction of NAD(P)⁺. *Organometallics* **1991**, *10*, 1568–1577. (b) Betanzos-Lara, S.; Liu, Z.; Habtemariam, A.; Pizarro, A. M.; Qamar, B.; Sadler, P. J. Organometallic Ruthenium and Iridium Transfer-Hydrogenation Catalysts Using Coenzyme NADH as a Cofactor. *Angew. Chem., Int. Ed.* **2012**, *51*, 3897–3900. (c) Maenaka, Y.; Suenobu, T.; Fukuzumi, S. Efficient Catalytic Interconversion between NADH and NAD⁺ Accompanied by Generation and Consumption of Hydrogen with a Water-Soluble Iridium Complex at Ambient Pressure and Temperature. *J. Am. Chem. Soc.* **2012**, *134*, 367–374. (d) Maenaka, Y.; Suenobu, T.; Fukuzumi, S. Hydrogen Evolution from Aliphatic Alcohols and 1,4-Selective Hydrogenation of NAD⁺ Catalyzed by a [C,N] and a [C,C] Cyclometalated Organoiridium Complex at Room Temperature in Water. *J. Am. Chem. Soc.* **2012**, *134*, 9417–9427. (e) Mayer, C.; Hilvert, D. A Genetically Encodable Ligand for Transfer Hydrogenation. *Eur. J. Org. Chem.* **2013**, *2013*, 3427–3431.

(29) Letko, C. S.; Heiden, Z. M.; Rauchfuss, T. B. Activation and Deactivation of Cp*Ir(TSDPEN) Hydrogenation Catalysts in Water. *Eur. J. Inorg. Chem.* **2009**, *2009*, 4927–4930.

(30) Soni, R.; Cheung, F. K.; Clarkson, G. C.; Martins, J. E. D.; Graham, M. A.; Wills, M. The Importance of the N-H Bond in Ru/TSDPEN Complexes for Asymmetric Transfer Hydrogenation of Ketones and Imines. *Org. Biomol. Chem.* **2011**, *9*, 3290–3294.

(31) Soldevila-Barreda, J. J.; Bruijninx, P. C. A.; Habtemariam, A.; Clarkson, G. J.; Deeth, R. J.; Sadler, P. J. Improved Catalytic Activity of Ruthenium–Arene Complexes in the Reduction of NAD⁺. *Organometallics* **2012**, *31*, 5958–5967.

(32) (a) Liu, Z.; Romero-Canelón, I.; Qamar, B.; Hearn, J. M.; Habtemariam, A.; Barry, N. P. E.; Pizarro, A. M.; Clarkson, G. J.; Sadler, P. J. The Potent Oxidant Anticancer Activity of Organoiridium Catalysts. *Angew. Chem., Int. Ed.* **2014**, *53*, 3941–3946. (b) Fu, Y.; Sanchez-Cano, C.; Soni, R.; Romero-Canelon, I.; Hearn, J. M.; Liu, Z.;

Wills, M.; Sadler, P. J. The Contrasting Catalytic Efficiency and Cancer Cell Antiproliferative Activity of Stereoselective Organoruthenium Transfer Hydrogenation Catalysts. *Dalton Trans.* **2016**, *45*, 8367–8378.

(33) Ngo, A. H.; Ibañez, M.; Do, L. H. Catalytic Hydrogenation of Cytotoxic Aldehydes Using Nicotinamide Adenine Dinucleotide (NADH) in Cell Growth Media. *ACS Catal.* **2016**, *6*, 2637–2641.

(34) (a) Oppelt, K. T.; Gasiorowski, J.; Egbe, D. A. M.; Kollender, J. P.; Himmelsbach, M.; Hassel, A. W.; Sariciftci, N. S.; Knör, G. Rhodium-Coordinated Poly(arylene-ethynylene)-*alt*-poly(arylene-vinylene) Copolymer Acting as Photocatalyst for Visible-Light-Powered NAD⁺/NADH Reduction. *J. Am. Chem. Soc.* **2014**, *136*, 12721–12729. (b) Soldevila-Barreda, J. J.; Habtemariam, A.; Romero-Canelón, I.; Sadler, P. J. Half-Sandwich Rhodium(III) Transfer Hydrogenation Catalysts: Reduction of NAD⁺ and Pyruvate, and Antiproliferative Activity. *J. Inorg. Biochem.* **2015**, *153*, 322–333. (c) Leiva, C.; Lo, H. C.; Fish, R. H. Aqueous Organometallic Chemistry. 3. Catalytic Hydride Transfer Reactions with Ketones and Aldehydes Using [Cp*Rh(BPy)(H₂O)](OTf)₂ as the Precatalyst and Sodium Formate as the Hydride Source: Kinetic and Activation Parameters, and the Significance of Steric and Electronic Effects. *J. Organomet. Chem.* **2010**, *695*, 145–150.

(35) Schafer, F. Q.; Buettner, G. R. Redox Environment of the Cell as Viewed through the Redox State of the Glutathione Disulfide/Glutathione Couple. *Free Radical Biol. Med.* **2001**, *30*, 1191–1212.

(36) Perry, G.; Raina, A. K.; Nunomura, A.; Wataya, T.; Sayre, L. M.; Smith, M. A. How Important Is Oxidative Damage? Lessons from Alzheimer's Disease. *Free Radical Biol. Med.* **2000**, *28*, 831–834.

(37) Trachootham, D.; Alexandre, J.; Huang, P. Targeting Cancer Cells by ROS-Mediated Mechanisms: A Radical Therapeutic Approach? *Nat. Rev. Drug Discovery* **2009**, *8*, 579–591.

(38) Fu, Y.; Romero, M. J.; Habtemariam, A.; Snowden, M. E.; Song, L.; Clarkson, G. J.; Qamar, B.; Pizarro, A. M.; Unwin, P. R.; Sadler, P. J. The Contrasting Chemical Reactivity of Potent Isolelectronic Iminopyridine and Azopyridine Osmium(II) Arene Anticancer Complexes. *Chem. Sci.* **2012**, *3*, 2485–2494.

(39) (a) Chen, F.; Romero-Canelón, I.; Soldevila-Barreda, J. J.; Song, J.-L.; Coverdale, J. P. C.; Clarkson, G. J.; Kasparkova, J.; Habtemariam, A.; Wills, M.; Brabec, V.; Sadler, P. J. Transfer Hydrogenation and Antiproliferative Activity of Tethered Half-Sandwich Organoruthenium Catalysts. *Organometallics* **2018**, *37*, 1555. (b) Chen, F.; Soldevila-Barreda, J. J.; Romero-Canelón, I.; Coverdale, J. P. C.; Song, J.-L.; Clarkson, G. J.; Kasparkova, J.; Habtemariam, A.; Brabec, V.; Wolny, J. A.; Schunemann, V.; Sadler, P. J. Effect of Sulfonamidoethylenediamine Substituents in RuII Arene Anticancer Catalysts on Transfer Hydrogenation of Coenzyme NAD⁺ by Formate. *Dalton Trans.* **2018**, *47*, 7178.

(40) (a) Marullo, R.; Werner, E.; Degtyareva, N.; Moore, B.; Altavilla, G.; Ramalingam, S. S.; Doetsch, P. W. Cisplatin Induces a Mitochondrial-Ros Response That Contributes to Cytotoxicity Depending on Mitochondrial Redox Status and Bioenergetic Functions. *PLoS One* **2013**, *8*, e81162. (b) Bragado, P.; Armesilla, A.; Silva, A.; Porras, A. Apoptosis by Cisplatin Requires p53 Mediated p38alpha MAPK Activation through ROS Generation. *Apoptosis* **2007**, *12*, 1733–1742.

(41) (a) He, L.; Liao, S.-Y.; Tan, C.-P.; Ye, R.-R.; Xu, Y.-W.; Zhao, M.; Ji, L.-N.; Mao, Z.-W. Ruthenium–arene– β -carboline Complexes as Potent Inhibitors of Cyclin-Dependent Kinase 1: Synthesis, Characterization and Anticancer Mechanism Studies. *Chem. - Eur. J.* **2013**, *19*, 12152–12160. (b) Spoerlein-Guettler, C.; Mahal, K.; Schobert, R.; Biersack, B. Ferrocene and (Arene)ruthenium(II) Complexes of the Natural Anticancer Naphthoquinone Plumbagin with Enhanced Efficacy against Resistant Cancer Cells and a Genuine Mode of Action. *J. Inorg. Biochem.* **2014**, *138*, 64–72. (c) Chow, M. J.; Licon, C.; Pastorin, G.; Mellitzer, G.; Ang, W. H.; Gaiddon, C. Structural Tuning of Organoruthenium Compounds Allows Oxidative Switch to Control Er Stress Pathways and Bypass Multidrug Resistance. *Chem. Sci.* **2016**, *7*, 4117–4124. (d) Kandlioller, W.; Balsano, E.; Meier, S. M.; Jungwirth, U.; Goschl, S.; Roller, A.; Jakupc,

M. A.; Berger, W.; Keppler, B. K.; Hartinger, C. G. Organometallic Anticancer Complexes of Lapachol: Metal Centre-Dependent Formation of Reactive Oxygen Species and Correlation with Cytotoxicity. *Chem. Commun.* **2013**, *49*, 3348–3350.

(42) Bennett, M. A.; Smith, A. K. Arene Ruthenium(II) Complexes Formed by Dehydrogenation of Cyclohexadienes with Ruthenium(III) Trichloride. *J. Chem. Soc., Dalton Trans.* **1974**, 233–241.

(43) (a) Dolomanov, O. V.; Bourhis, L. J.; Gildea, R. J.; Howard, J. A. K.; Puschmann, H. OLEX2: A Complete Structure Solution, Refinement and Analysis Program. *J. Appl. Crystallogr.* **2009**, *42*, 339–341. (b) Sheldrick, G. A Short History of SHELX. *Acta Crystallogr., Sect. A: Found. Crystallogr.* **2008**, *64*, 112–122. (c) Sheldrick, G. SHELXT - Integrated Space-Group and Crystal-Structure Determination. *Acta Crystallogr., Sect. A: Found. Adv.* **2015**, *71*, 3–8.